



Controlled synthesis of graphene via electrochemical route and its use as efficient metal-free catalyst for oxygen reduction



Nathanael Komba, Qiliang Wei, Gaixia Zhang, Federico Rosei*, Shuhui Sun*

Institut National de la Recherche Scientifique-Énergie Matériaux et Télécommunications, Varennes, QC J3X 1S2, Canada

ARTICLE INFO

Keywords:

Electrochemical exfoliation
Electrolyte
Graphite plate
Graphite foil
Oxygen reduction reaction

ABSTRACT

The oxygen reduction reaction (ORR) is a critical step in the operation of fuel cells. The exploration of efficient, low cost and durable non-precious ORR catalysts, to replace the rare and expensive Pt-based catalysts, is promising towards the large-scale commercialization of fuel cells. Here, we report the fabrication of high-quality graphene (GP) with controllable layers, using a simple, versatile and cost-effective electrochemical exfoliation method. Our systematic studies revealed that the graphite precursor, electrolyte temperature, and pyrolysis conditions largely affect the number of layers and quality of the graphene, which consequently has a significant effect on its ORR performance. The optimized graphene sample was subsequently heat-treated in the NH₃ atmosphere to obtain the nitrogen-doped graphene (N-GP). As a metal-free electrocatalyst, N-GP exhibit much enhanced ORR activity than GP, and comparable ORR activity to the state-of-the-art Pt/C catalyst. Moreover, it also shows better stability than Pt/C catalyst in alkaline solution.

1. Introduction

The oxygen reduction reaction (ORR) is a fundamental process in energy conversion devices such as fuel cells [1] and energy storage technologies such as metal-air batteries [2,3]. The ORR is a cathodic process which plays a critical role in the overall performance of a fuel cell. In aqueous solution, the ORR is a slow and highly irreversible process [4,5]. Due to the inherent nature of the sluggish kinetics of ORR, the demand for highly efficient electrocatalysts is indispensable to improve the performance of fuel cells.

Currently, platinum (Pt) based catalysts are the only commercially available efficient catalysts for fuel cells. However, the high cost and low abundance of Pt hinder the wide-spread commercialization of hydrogen fuel cells [6,7]. In addition, in normal test conditions, Pt-based catalysts suffer from susceptibility to methanol cross-over, carbon monoxide poisoning, carbon corrosion and Pt particles agglomeration [8]. Considerable efforts have been directed towards 1) decreasing Pt content in the catalysts by developing either Pt-metal alloy or novel support materials and 2) replacing Pt-based catalysts by either non-precious metal [9] or metal free materials [10–12]. In particular, the exploration of highly efficient and inexpensive metal-free electrocatalysts for the ORR is being widely investigated [13]. Among various alternatives, graphene is an emerging and promising candidate for a metal-free catalyst to replace Pt, especially in alkaline media.

Graphene, a two-dimensional sheet of carbon atoms covalently bonded into a hexagonal lattice matrix, displays unique physicochemical properties, such as large surface area, high electronic conductivity, and excellent chemical stability [14–16]. These extraordinary features may be useful for many potential applications such as electronic devices, transparent electrodes, catalysis, energy storage and conversion [17–19]. Moreover, it has been shown that the catalytic activity of graphene can be increased significantly by doping it with heteroatoms such as N and S atoms [15,16,20,21]. Accordingly, when graphene is doped with N-atoms, it is found to have excellent electrocatalytic activity towards ORR in alkaline media.

The specific method used to prepare graphene is also important for ORR electrocatalysis, as it is closely related to the quality, yield, and efficiency of the final product, as well as its production cost. Therefore, methods that preserve the inherent properties of graphene, while avoiding the use of any hazardous chemical/condition, are highly desired [22,23]. However, in the most traditional Hummer's method for the preparation of graphene, strong mineral acids and oxidizing agents are used, causing several manufacturing challenges which are not easy to address [24,25]. On the other hand, for ORR applications, catalysts with high surface area, excellent electronic conductivity, and balanced, functional groups are highly desired. Although perfect reduced graphene oxide (r-GO) inherently has high surface area and excellent conductivity, its hydrophobic nature causes challenges such as

* Corresponding authors.

E-mail addresses: rosei@emt.inrs.ca (F. Rosei), shuhui@emt.inrs.ca (S. Sun).

electrode wettability, thereby decreasing the ORR performance [26]. On the other hand, the highly hydrophilic graphene oxide shows poor conductivity, which is unfavorable for ORR. Therefore, a method that could lead to high-quality graphene with well-balanced catalytic properties is highly desirable. In this context, electrochemical exfoliation is a promising method for the preparation of graphene for ORR electrocatalysis. The electrochemical approach potentially has many advantages over traditional chemical methods, including its being simple, easily scalable, and cost-effective, and most importantly allowing the tuning of the level of oxidation [25,26]. Graphene exfoliated using electrochemical methods are of high quality, with a few defects.

In this work, taking advantage of the electrochemical exfoliation method, we use two types of raw materials, i.e., graphite plate and graphite foil, to prepare high-quality graphene under different reaction conditions. Systematic studies revealed that N-doping was successfully achieved with pyridinic nitrogen dominance. The ORR activity of the catalysts varied significantly with the exfoliating and post-exfoliation conditions. The optimal N-doped graphene exhibits comparable ORR performance to commercial Pt/C catalysts. Our work suggests that the low cost and environmentally friendly electrochemical method is a potentially viable approach to prepare graphene with excellent ORR activity.

2. Experimental

2.1. Materials

Graphite plate (99%) and foils (0.5 mm, 99.8%) were purchased from Alfa Aesar, Fischer Scientific. Ammonium sulfate ($(\text{NH}_4)_2\text{SO}_4$, 99%), Polyvinylpyrrolidone (average molecular weight 40,000) (99%), 2,2,6,6-Tetramethyl-1-piperidinyloxy, (TEMPO) (98%), platinum on Vulcan (20%, XC-72R; E-TEK), potassium hydroxide (KOH) and reagent alcohol, were purchased from Sigma-Aldrich. All chemicals were of analytical grade and used without further purification.

2.2. Electrochemical exfoliation and nitrogen functionalization of graphene

The exfoliation of graphene (GP) was carried out using a DC power supply in a two-electrode cell as reported elsewhere with slight modification [22,24,25]. In a typical synthesis, a graphite substrate served as a positive electrode, and Pt wire acted as a negative electrode in an electrochemical cell filled with $(\text{NH}_4)_2\text{SO}_4$ (0.1 M) aqueous solution. A constant biased potential of ± 10 V was applied between the two electrodes. The exfoliation of graphene was achieved at room temperature (~ 22 °C) and in some cases carried out at different temperatures (22, 40, 60, and 80 °C) in a heated water bath. The duration of the exfoliation process was found to depend on the graphite source, the concentration of the electrolyte and the applied bias potential. To gain insights on the quality of the exfoliated graphene, different doses of an organic reagent, TEMPO was added to some recipes. The exfoliation scheme of graphite is shown in Fig. 1. The as-exfoliated product was collected, washed thoroughly with deionized water and reagent alcohol by vacuum filtration, and then dispersed in water by sonication for 15 min. The graphitic particles which are not exfoliated were separated from graphene by centrifuging the dispersion at 1000 rpm for 10 min. The fine suspension in the upper part of the centrifuge tube was fractionated into components with different graphene layers by controlling the centrifugation speed from 2500 rpm (to get multi-layers), 5000 rpm (to get thin layers) to 14,000 rpm (to obtain very thin layers). The graphene powders were obtained by freeze-drying. The obtained graphene was functionalized with nitrogen atoms by heating the graphene powders at 950 °C in argon for 60 min and then in ammonia (NH_3) for 15 min to obtain nitrogen-doped graphene (N-GP).

2.3. Physical characterization

The structural morphologies and composition of the catalysts were characterized using transmission electron microscopy (TEM, JEOL JEM-2100 F operated at 200 kV), field emission scanning electron microscopy (FE-SEM) and X-ray photoelectron spectroscopy (XPS) using a VG (Escalab220i - XL) equipped with Al K_α line as an excitation source. The electronic structure was investigated using a UV-vis absorption spectrophotometer (thermos scientific Nanodrop 2000c).

2.4. Electrochemical characterization

The catalyst ink was prepared by dispersing 10 mg of the catalyst to the solution of ethanol (350 μl) and Nafion ionomer (95 μl , 5 wt %), followed by two cycles of 15 min sonication and agitation in a vortex shaker. This ink, then casted on the disc part of the rotating ring disc electrode (RRDE, 5.61 mm diameter glassy carbon disk and Pt ring) or the 5.0 mm diameter glassy carbon rotating disc electrode (RDE), with a catalyst loading of 0.8 mg cm^{-2} . For comparison, 20 wt% Pt/C catalyst (E-ETK) was prepared through the same procedure with a loading amount of $100 \mu\text{g}/\text{cm}^2$ ($20 \mu\text{g}_{\text{Pt}}/\text{cm}^2$). All electrochemical measurements were carried out in a three-electrode cell at room temperature using the Autolab electrochemical system (Model, PGSTAT-302, Ecochemie, Brinkman Instruments). In all experiments, Pt wire and mercury/mercury oxide (Hg/HgO) was used as the counter electrode (CE) and a reference electrode (RE), respectively. The ORR activity of the graphene catalysts was evaluated in O_2 saturated 0.1 M KOH solution with scan rates of 50 mV s^{-1} and 10 mV s^{-1} for cyclic Voltammetry (CV) and linear sweep voltammograms (LSVs), respectively, recorded in the range of 0–1.2 V. To record LSVs, the electrode was rotated at 1600 rpm. The potentials in this work are normalized to the reversible hydrogen electrode (RHE). The peroxide yield ($\text{H}_2\text{O}_2\%$) and the electron transfer number (n) were calculated using a ring, disk currents (I_r, I_d) and the estimated collection efficiency ($N = 0.37$) using Eqs. (1) and (2). To investigate the stability of the catalysts accelerated degradation testing (ADT) were performed in the oxygen-saturated 0.1 M KOH between 0.6 and 1.0 V vs. RHE at 100 mV s^{-1} . The LSV tests were carried in the oxygen-saturated electrolyte at the beginning and end of each ADT to evaluate the effect of the cycles on catalytic activity.

$$\text{H}_2\text{O}_2\% = \frac{200 \times I_r}{NI_d + I_r} \quad (1)$$

$$n = \frac{4 \times I_d}{I_d + I_r/N} \quad (2)$$

3. Results and discussion

It is widely accepted that a complete electrochemical exfoliation of graphite begins with the oxidation of graphite edges and grain boundaries, followed by intercalation of water molecules and electrolyte ions when a bias potential is applied [22,25,27,28]. The electrolysis of the intercalated species produces some gaseous products which cause the expansion of graphitic layers and consequently separation into particles with loosely attached layers or individual sheets of graphene [27,28]. However, the mechanism of the exfoliation steps could be slightly different depending on the type of the graphite raw material. For example, as shown in Fig. S1, during the exfoliation of graphite foils, we observed only the expansion of graphite foil using a static bias potential of -10 V for five minutes. For both processes, expansion, and exfoliation were observed when the bias potential was $+10$ V for similar duration. This observation can be accounted by the degree of compaction of the two kind of graphite substrates and the mechanism of exfoliation. The graphite plate is made of fine grain, with high strength and density graphite as well as high degree of compaction, it is very hard compared to the soft nature of the graphite foils. In the mechanism

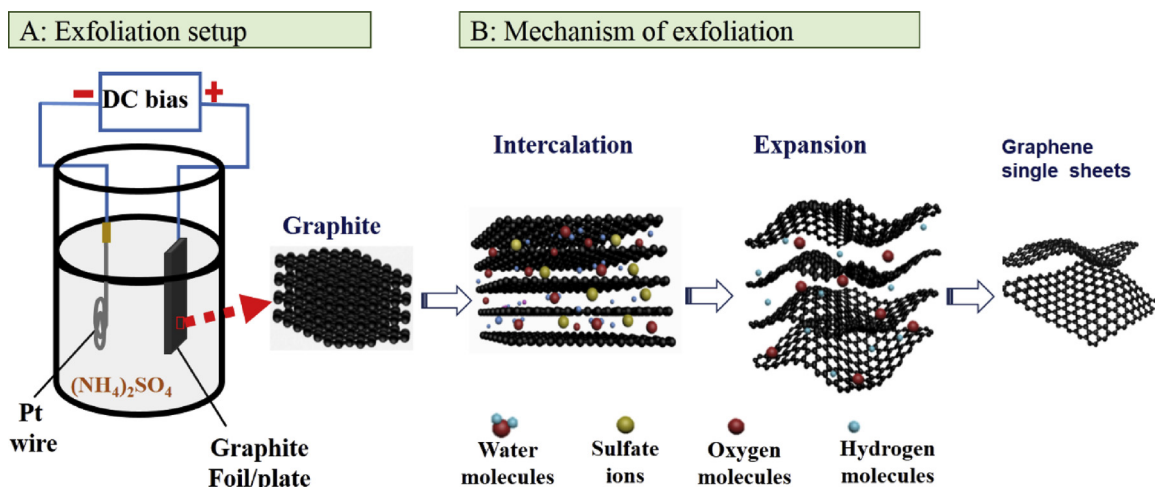


Fig. 1. Schematic illustration of the setup for the electrochemical exfoliation production of graphene, and the exfoliation mechanism in aqueous $(\text{NH}_4)_2\text{SO}_4$ solution.

of graphite exfoliation, there are three suggested key processes; (i) oxidation of the edge sites and grain boundaries, (ii) intercalation of ions within the graphitic layers, and (iii) expansion and separation [25,28]. Generally, in the optimized conditions of exfoliation of graphite foils, we applied a bias potential of +2.5 V for wetting, then ramped up to +10 V for oxidation of edges, intercalation, and exfoliation. Afterwards, -10 V is applied for the reduction of oxidized groups [25]. Due to the soft nature of the graphite foil, during the wetting process (by application of +2.5 V), some of the electrolytes ions and water molecules easily intercalate into the layers of graphite foils. Since the graphite edges are not oxidized, when a bias potential is changed to -10 V, the reduced gaseous products of the electrolysis only causes the expansion of the graphite foil, but the force is not enough to cause separation of the graphene sheet. However, when a bias potential of +10 V is applied after wetting, all three key processes happen in sequence, i.e., the exfoliation is initiated by oxidation of graphite edges, followed by the intercalation, expansion (electrolysis of gaseous products) and separation to graphene. On the other hand, the alternation of -10/+10 V voltages was necessary to achieve the exfoliation of graphite sheets using a graphite plate as a precursor. The difference in the mechanism of exfoliation is probably caused by the different compact degree and level of order of the graphite used.

The morphologies of as-synthesized graphene samples were investigated by TEM. Fig. 2 shows typical TEM images of graphene exfoliated from a graphite foil (Fig. 2a–c) and graphite plate (Fig. 2d–f). The graphene sheets from both graphite sources appear to be uniform and very thin, about two to a few layers, as observed by counting the folded edges of the HRTEM images (Fig. 2b, e). The higher magnification images in Fig. 2(b, e) indicate that the graphene sheets are very thin, and the folded edges reveal that the graphene is only a few layers. Fig. 2(c) and (f) are the corresponding selected area electron diffraction (SAED) patterns, indicating the single crystalline lattice structure with a characteristic hexagonal diffraction pattern of few layers graphene obtained from both graphite sources [27,29].

However, there are some slight differences when using different graphite precursors. For example, very uniform, large piece and ultra-thin (1–2 layers) graphene sheets are obtained when the graphite foil is used, while smaller pieces with non-uniform thickness graphene sheets are obtained when the graphite plate is used (as shown in Fig. 2a and d). The degree of crystallinity is higher for the graphene that is exfoliated from graphite foil than the graphite plate. This could be attributed to the longer exfoliation time when the graphite plate is used, compared to graphite foils. The exfoliation process, using a graphite plate as precursor took about one hour or longer to obtain a significant amount of graphene produce, while it only takes 3–5 min to complete

the process when using a graphite foil. The long exfoliation time of graphite plate imparts the as-exfoliated graphene to a longer oxidizing environment, resulting in the formation of relatively small pieces with a large number of oxidized functional groups. The selected area electron diffraction (SAED) features with less well-defined diffraction spots (Fig. 2f), confirms the poor crystalline structure of the GPP [30]. The SEM images in Fig. S2 show that the surfaces of the as-exfoliated graphene are thin and smooth with wrinkled features.

UV-vis absorption spectroscopy was performed to determine the extent of the oxidized carbon atoms which occurred during the exfoliation process. Fig. 3 shows the UV-vis absorption spectra of the graphene samples exfoliated in an electrolyte containing different doses of reducing agent, TEMPO. The absorption peak of the as-exfoliated graphene in an electrolyte without TEMPO is observed at around 257 nm, and gradually redshifted to about 270 nm as the amount of TEMPO increased from zero to 0.96 mmol. The observed shifts in the absorption peak can be attributed to the restoration of C-C sp^2 hybridization within the graphene lattice structure. The absorption peak maximum for the graphene oxide is reported to be around 231 nm while that of the reduced graphene oxide occurs at ca. 271 nm [22,31]. The absorption in this region (270 nm) arises from the excitation π -plasmon resonance in the graphene structure [31–33]. Therefore, the occurrence of the absorption peak at ca. 257–270 nm for the as-exfoliated graphene further confirms the production of graphene with a controllable degree of oxidation by means of electrochemical exfoliation methods.

The chemical composition of the graphene samples was probed by X-ray photoelectron spectroscopy (XPS). Fig. 4 displays the XPS spectra of as-exfoliated graphene (GPP) and nitrogen doped graphene (N-GPP). The survey spectra are shown in Fig. 4a suggests that the as-exfoliated graphene contains a strong and prominent C 1 s peak and relatively small O 1 s peak, indicating fewer oxygen-containing functional groups. The oxygen content in the GPP measured by XPS is 5 at% leading to a calculated ratio of C/O to be 19. The high ratio of C/O implies that the as-exfoliated graphene has a high degree of sp^2 carbon [25,32,34]. On the other hand, the survey spectrum of the N-GPP indicates the presence of N 1 s peak in addition to C 1 s and O 1 s peaks, suggesting the successful doping of N atoms into the GPP during pyrolysis at 950 °C in NH_3 for 15 min. The surface concentration of C 1s, N 1s, and O 1s in the N-GPP as estimated is 96.7 at%, 2.0 at% and 1.5 at%, respectively. The decreased oxygen content for the N-GPP is attributed to the decomposition of carboxyl functional groups during pyrolysis and replacement of oxygen by nitrogen bonded to carbon. As shown in Fig. 4b, the presence of the C 1 s peak with the main component at 284.6 eV for $\text{C}=\text{C}$, minor peaks at 285.5 eV for $\text{C}-\text{O}$ and 286.7 eV for $\text{C}=\text{O}$ in the as-exfoliated GPP is a signature of the low level of oxidized species in the

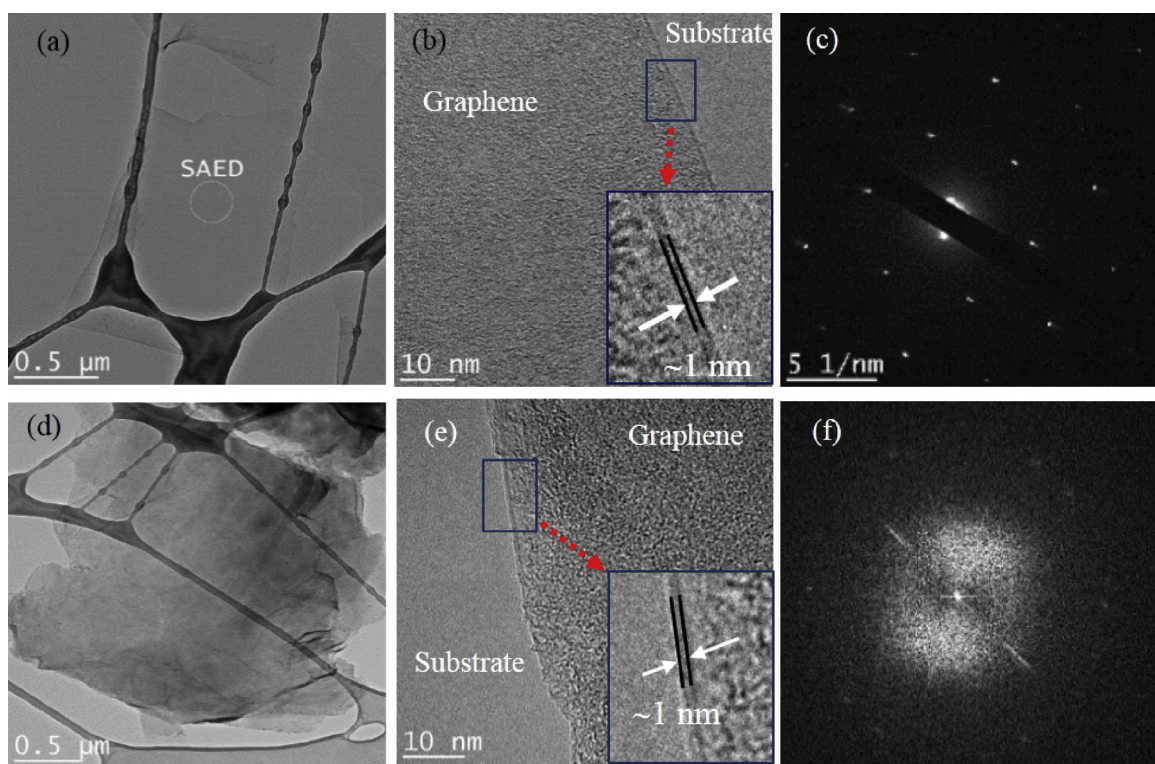


Fig. 2. TEM images and selected area electron diffraction (SAED) of typical graphene samples exfoliated from graphite foils and plates. (a–c) Graphite foil graphene (GPF). (d–e) Graphene of graphite plate (GPP). The grapheme from both graphite sources are few-layer, uniform, and have a well-defined crystalline structure.

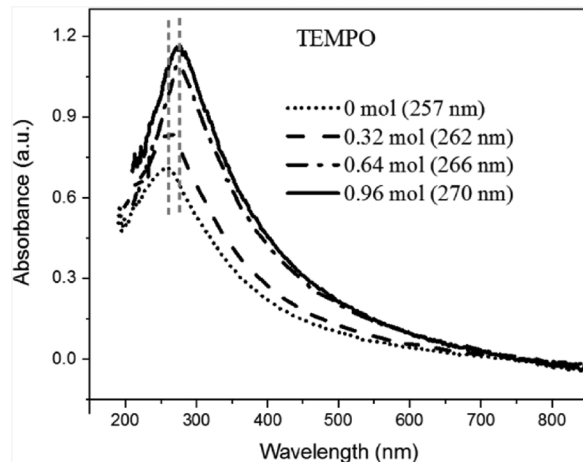


Fig. 3. UV-vis absorption spectra are showing absorption peaks of the graphene samples prepared in 0.1 M $(\text{NH}_4)_2\text{SO}_4$ electrolyte containing different doses of organic reducing agent 2,2,6,6-Tetramethylpiperidine-1-oxyl (TEMPO). The reducing agent was added to reduce part of the functional groups introduced during exfoliation.

graphene lattice structure [25,35]. The C 1 s peak for N-GP (Fig. 4c) can be deconvoluted into four peaks, corresponding to C=C (284.6 eV), C=N (285.5 eV), C-N (286 eV), and C=O (287 eV), respectively. It is well established that the charge distribution in the C atoms in the N-doped carbon matrix can be influenced by the neighboring N dopants, which serve as a potential active center for ORR [36]. In addition, Fig. 4d shows the deconvolution of the N 1 s peak into four components corresponding to different N atom configurations. The components are assigned to pyridinic-C-N (398.3 eV, 71 at %), pyrrolic-C-N (400.2 eV, 9 at %), graphitic-C-N (401 eV, 16 at %), and oxidized-N (402.7 eV, 4 at %). The N-doped graphene contains the highest composition of pyridinic-C-N which contributes one π electron to the π system of graphene. This

phenomenon is believed to be able to enhance the ORR activity of the N-doped graphene [19,31,37,38].

The LSV experiments were performed to evaluate the ORR activity of the as-exfoliated graphene from graphite foil (GPF) and plate precursors (GPP) and NH_3 -treated graphene (exfoliated from the graphite plate, N-GPP). The ORR activity of the catalysts was evaluated by the exhibition of the highest possible positive value of the onset potential, half-wave potential ($E_{1/2}$) or current density at 0.80 V vs. RHE. Fig. 5 shows the typical ORR polarization curves, the corresponding calculated electrons transfer number and percentage peroxide produced for the as-exfoliated GPF, GPP and N-GPP catalysts. The GPP exhibited superior positive onset potential (0.82 V vs. RHE), the half-wave potential (0.75 V) and current density at 0.80 V (0.34 mA cm^{-2}) as compared to 0.78 V, 0.67 V and 0.04 mA cm^{-2} respectively, of the GPF. The as-exfoliated GPP displayed better ORR performance in 0.1 M KOH solution than the graphene prepared by other methods, e.g., three-dimensional (3D) graphene [39,40], nanosheets by grinding high purity graphite in ionic liquid [14,41], edge-functionalized graphene by ball milling [26], and reduced graphene oxide by Hummer's method [42,43]. Detailed comparison is given in Table S1. The improved ORR performance of GPP is ascribed to the presence of numerous functionalized edges available for the adsorption and dissociation of O_2 in addition to the efficient electron transfer between the electrode and the high structural crystalline quality of its basal plane [36,44,45]. The abundance of the edges of the former possibly originates from the exfoliation process. The duration of the exfoliation process for the graphite plate was long (one to a few hours), compared to the graphite foil (3–5 min). The extended period of the exfoliation process subjects the edges of graphene to further oxidation, consequently leading to the formation of more functional groups. The functionalized edges of graphene render the hydrophilic nature of the modified electrode, facilitating the diffusion of oxygen, thereby providing more active centers [26,45,46]. The ORR activity of the GPP is further enhanced by the pyrolysis of the sample in NH_3 at 950 °C (named as N-GPP). The high-temperature pyrolysis in NH_3 introduces N-atoms into the graphene

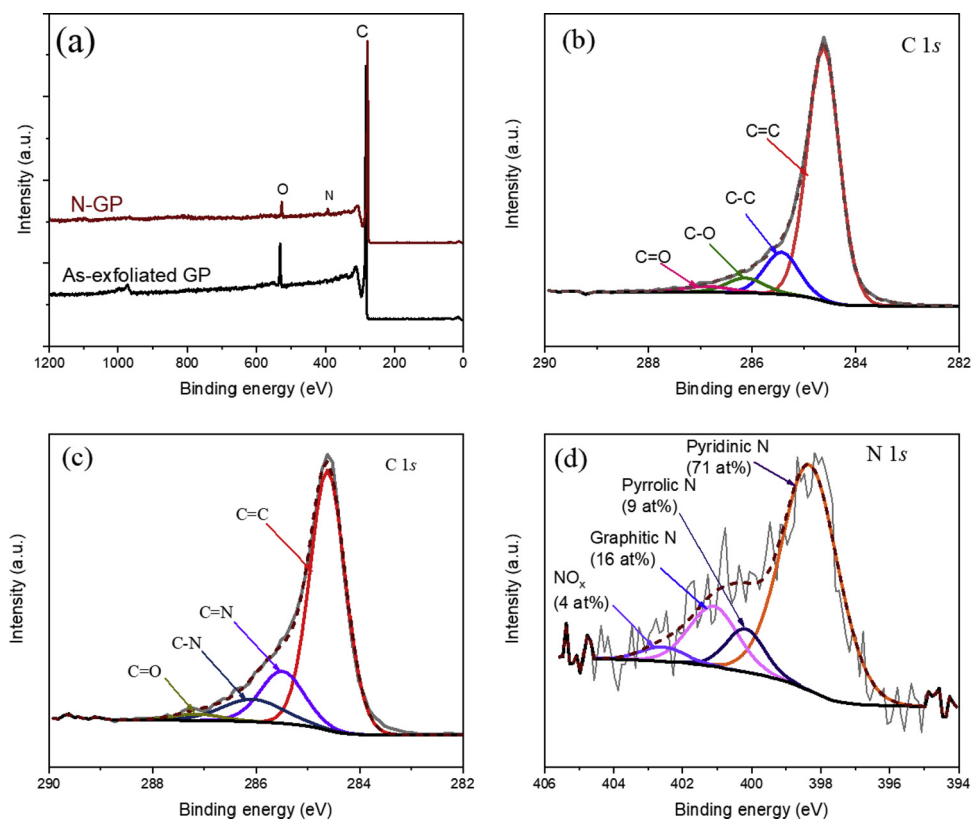


Fig. 4. XPS spectra of graphene exfoliated from a graphite plate (GPP) (a) survey of as-exfoliated graphene (GP) and N-doped graphene (N-GP) and high-resolution C 1s spectrum of (b) as-exfoliated GPP, and (c) N-GP, and (d) high-resolution N 1s spectrum of the N-GP.

lattice matrix, which in turn causes the change of the charge distribution and electronic properties of the neighboring carbon atoms, hence increasing the probability of adsorption of oxygen molecules [19,36]. The increased ORR activity of the N-GP is evidenced by the more positive shifts of both half-wave (0.83 V vs. RHE) and onset (0.96 V) potentials, as well as the current density at 0.80 V (3.0 mA cm^{-2}). The enhanced activity is also revealed by the increase of the electron transfer number (above 3.5) and the relatively low production of hydrogen peroxide, H_2O_2 , (below 15%) in the potential range of 0.20–0.70 V, as seen in Fig. 5b. Therefore, it is apparent that graphite precursors and pyrolysis of graphene samples in NH_3 significantly

influence the ORR activity of the exfoliated catalysts.

Subsequently, we studied the temperature effect of the exfoliation electrolyte on the ORR performance of the graphene samples. Fig. 6a shows digital photos of the exfoliation products in the electrolytes (upper) and on the graphite substrates (lower) after 5 min of exfoliation, at different electrolyte temperatures. The exfoliation speed/efficiency is observed to decrease when the temperature increases. For example, at room temperature ($\sim 22^\circ\text{C}$), the largest amount of graphene was produced (upper image in Fig. 6a). This can also be supported by the largest consumption of the graphite substrate at $\sim 22^\circ\text{C}$ while the least consumption occurs at 80°C (lower image in Fig. 6a).

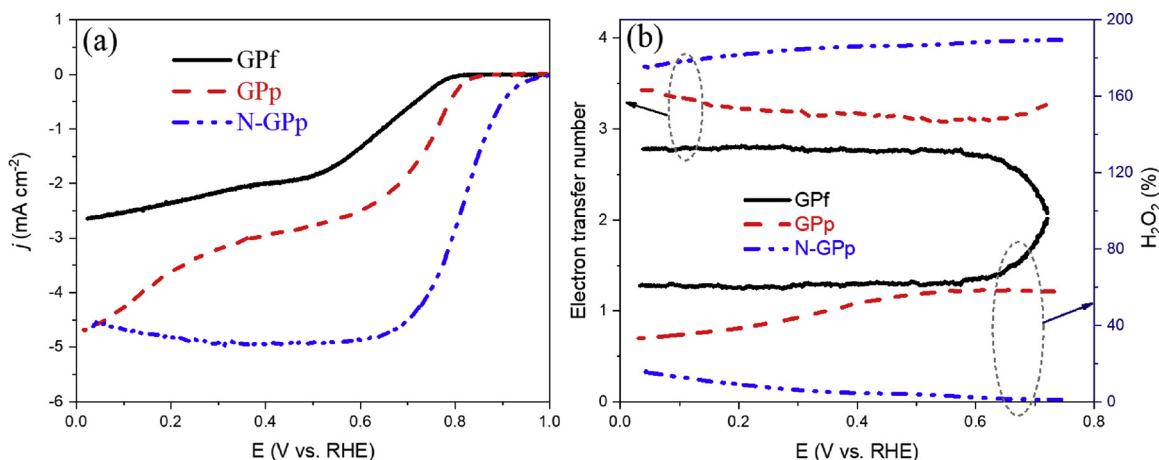


Fig. 5. ORR polarization curves of (a) as-exfoliated graphene from graphite foil (GPF, black line) and graphite plate (GPP, red line), and N-doped graphene (N-GPP, blue line), (b) The calculated electron transfer number, and peroxide production in the three catalysts. The measurements were carried out in N_2 , or O_2 saturated 0.1 M KOH, scan rate: 10 mV/s at 1600 rpm. (For interpretation of the references to colour in this figure legend, the reader is referred to the web version of this article).

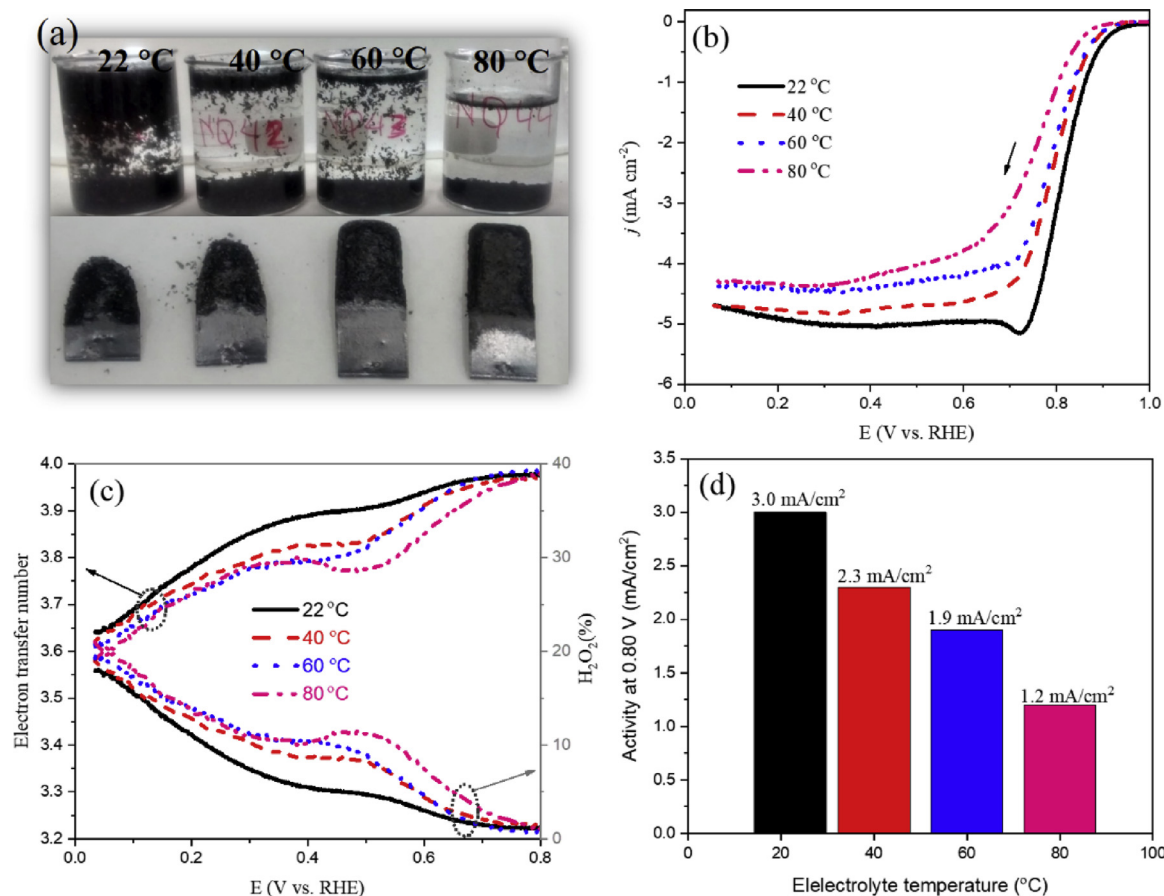


Fig. 6. (a) Digital images of as-exfoliated graphene products (in the beakers) and their corresponding graphite substrates after 5 min of exfoliation at 22, 40, 60 and 80 °C, respectively. (b) ORR polarization curves ranging from 0 to 1.0 V of the graphene (N-GPp) exfoliated at four different electrolyte temperatures, followed by pyrolysis in Ar at 1050 °C for 1 h and NH₃ for 15 min. The corresponding calculated (c) electron transfer number and (d) peroxide produced for the catalysts. Electrolytes: 0.1 M KOH, scan rate: 10 mV/s and rotation: 1600 rpm.

After exfoliation at various temperatures, the as-synthesized GPp samples were heat treated in Ar atmosphere at 1050 °C for 1 h and then in NH₃ for 15 min, to obtain N-GPp catalysts. The ORR performance of these N-GPp catalysts also decreases with the increasing temperature of the electrolyte, as shown in Fig. 6(b-d). Among all the N-GPp samples obtained at different temperatures, the sample exfoliated at 22 °C exhibited the best ORR activity in terms of highest half-wave (0.82 V) and onset (0.94 V) potentials, electron transfer number (above 3.8), and current density (3.0 mA/cm²) at 0.80 V, as well as the lowest peroxide yield (below 11%). The performance parameters of all N-GPp catalysts are summarised in Table S2. The higher density of the defects on the graphene obtained at a lower temperature may be responsible for its better ORR activity [47]. Our results are consistent with their observations. Furthermore, the graphene samples exfoliated at different temperatures display similar ORR kinetics as evidenced by the close Tafel slopes (Fig. S3) at the lower overpotential region. We believe that the presence of a suitable number of defects in the graphene edges could improve the hydrophilicity of the graphene, which, in turn, facilitates the adsorption of O-atoms in neighboring C-atoms while maintaining excellent electronic conductivity.

In addition, we studied the influence of the number of graphene layers, the pyrolysis temperature in NH₃, the sonication time, and the concentration of exfoliation electrolyte on the ORR activity of the graphene samples, and the results are summarised in Fig. 7. Before the ORR performance test, all the GPp samples underwent pyrolysis at 950 °C in an argon atmosphere for one hour and NH₃ for 15 min, except for two samples (at 750 °C and 1050 °C, respectively) in Fig. 7b, forming N-GPp samples. Fig. 7a shows that the ORR activity of the catalysts

follows the following order: few layers N-GPp > thin layers N-GPp > multilayers N-GPp. The enhanced activity of few layers N-GPp originates from the abundance of edges sites (capable of promoting the adsorption of O₂ molecules) and efficient electron transfer between the electrode's surface and the edges [14]. To study the effect of the pyrolysis temperature in NH₃, the thin layers GPp was used as reference material and annealed in NH₃ for 15 min at 750 °C, 950 °C and 1050 °C, respectively. As shown in Fig. 7b, the current density at 0.80 V significantly increased from 0.5 mA/cm⁻² for the sample at 750 °C to 1.9 mA/cm⁻² for the sample at 1050 °C. The increase in ORR activity can be attributed to the fact that the higher N amount was doped into the graphene lattice at higher NH₃ pyrolysis temperature, providing more active sites [11]. Furthermore, the influence of the sonication time was investigated as it is an integral step in the post-exfoliation treatment of the products. As shown in Fig. 7c, a significant enhancement of the ORR activity of the catalysts is observed when the sonication was prolonged from 5 min. to 120 min. The enhancement in the activity is caused by the introduction of more defects (active sites) in the graphene structure as the sonication time was extended. In addition, the concentration of exfoliation electrolyte also displayed a significant influence in the ORR activity of the N-GPp samples. As shown in Fig. 7d, the N-GPp derived from graphene exfoliated at 1.0 M (NH₄)₂SO₄ exhibited superior ORR activities than the one at 0.1 M (NH₄)₂SO₄. We anticipate that at high concentration of the electrolyte, the oxidation process of graphite edges is fast and the graphene produced is, accordingly, have more edge defects which in turn acts as the active sites for the ORR.

Finally, to investigate the stability of the N-GPp and 20% Pt/C

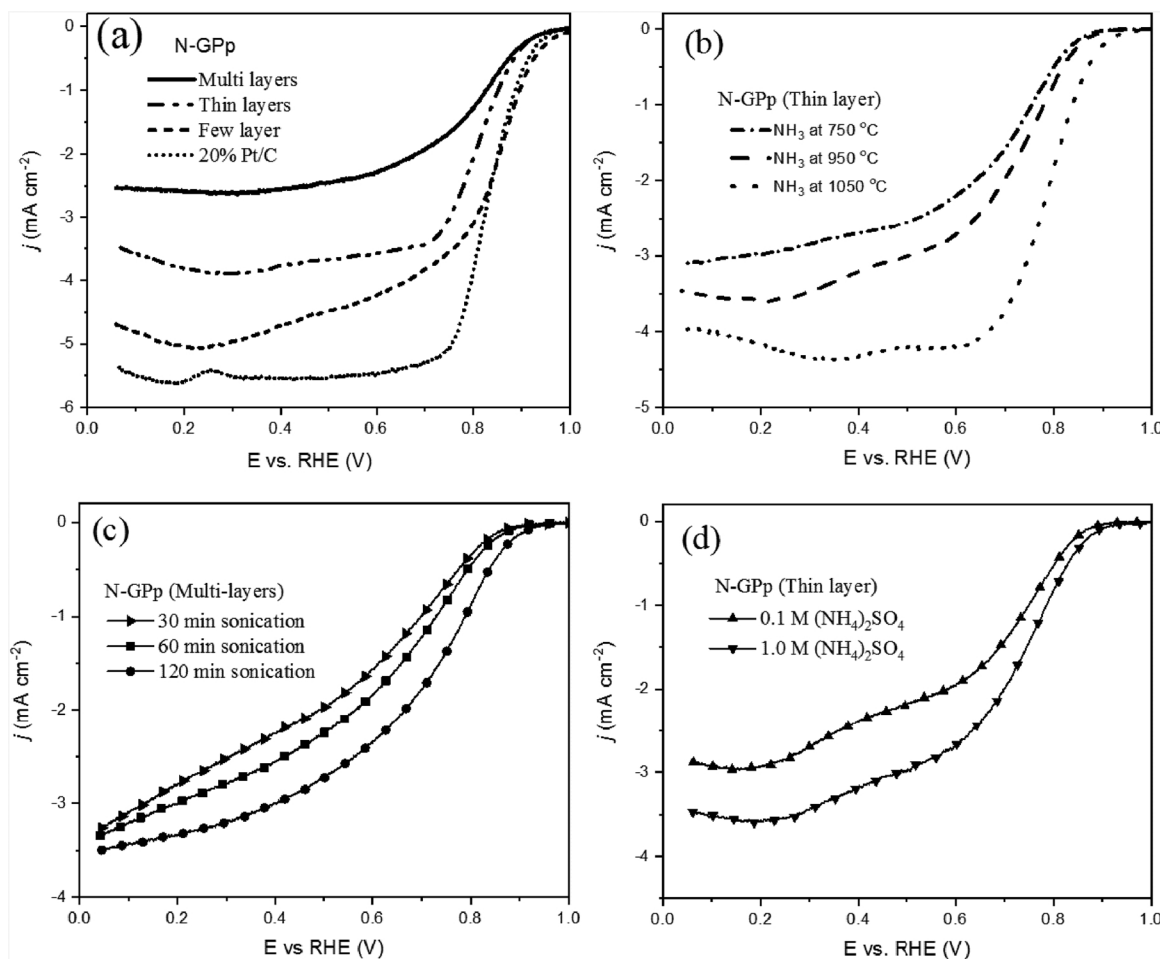


Fig. 7. The LSVs curve of N-GPp catalysts. (a) with different layers, (b) after different temperatures of pyrolysis in NH₃ (c) sonication for different duration. (d) Exfoliated in 0.1 M and 1.0 M (NH₄)₂SO₄ electrolytes. All LSV measurements were carried out in 0.1 M KOH media, scan rate: 10 mV/s, rotation speed: 1600 rpm.

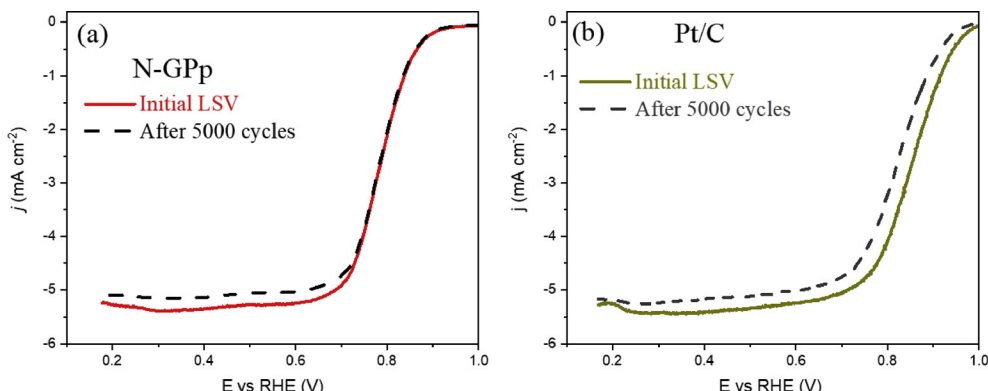


Fig. 8. Long-term performance of the catalysts (before and after ADT test, 5000 cycles). LSVs (a) few layer N-GPp and (b) 20% Pt/C recorded at 10 mV/s and 1600 rpm in O₂-saturated 0.1 M KOH at room temperature.

catalysts towards ORR, ADT was performed by continuous potential cycling between 0.6 and 1.0 V in O₂-saturated 0.1 M KOH, for 5000 potential cycles with a scan rate of 200 mV s⁻¹. As shown in Fig. 8, the N-GPp displayed exceptional durability. After 5000 consecutive CV cycles, the N-GPp catalysts showed almost superimposed LSVs before and after the ADT cycling. In contrast, the half-wave potential of the 20%Pt/C electrode significantly reduced by 30 mV after 5000 potential cycles under identical conditions. This observation suggests that N-GPp is more stable than the commercial Pt/C catalyst for ORR in alkaline media, which can be attributed to the strong covalent bonds between

the active sites and the graphitic lattice, as well as the high corrosion resistance of graphene.

4. Conclusions and perspectives

High-quality graphene with a controllable number of layers was successfully fabricated by a facile and inexpensive electrochemical method, using a low-cost graphite foil and plates as precursors in an aqueous electrolyte. In general, both graphite precursors generated thin and highly uniform graphene. We found that the ORR activity of

graphene exfoliated from the graphite plate was higher than the graphene obtained from the graphite foil. Further, as-synthesized graphene samples were converted into N-doped graphene (N-GPp) after NH₃ pyrolysis, which exhibits a highly enhanced ORR performance compared to pristine graphene, due to N-doping. Moreover, the N-GPp exhibited comparable ORR activity and better stability than the state-of-the-art commercial Pt/C catalyst. In addition, we found that the ORR activity of exfoliated graphene is influenced by the exfoliation and post-exfoliation parameters such as the temperature of the exfoliation electrolyte, the number of layers of graphene, pyrolysis temperature and concentration of the electrolyte. Therefore, it is possible to fine-tune the ORR activity of the graphene and N-GPp by manipulating the experimental parameters. Thus, we believe the N-GPp which can be prepared by a cost-effective method using low-cost precursors is a potential candidate of ORR catalyst in an alkaline fuel cell.

Author contributions

The manuscript was written through contributions of all authors. All authors have given approval to the final version of the manuscript.

Notes

The authors declare no competing financial interest.

Acknowledgments

S.S. and F.R. acknowledge individual Discovery Grants from the Natural Sciences and Engineering Research Council of Canada (NSERC), as well as funding from the Fonds de recherche du Québec - Nature et Technologies (FRQNT), le Centre Québécois sur les Matériaux Fonctionnels (CQMF), the Canada Foundation for Innovation (CFI). N.K. is grateful to the UNESCO Chair in Materials and Technologies for Energy Conversion, Saving and Storage (MATECSS) for a Ph.D. Excellence Scholarship. S. S. acknowledges the support from ECS Toyota Young Investigator Fellowship.

Appendix A. Supplementary data

Supplementary material related to this article can be found, in the online version, at doi:<https://doi.org/10.1016/j.apcatb.2018.10.070>.

References

- [1] C. Song, J. Zhang, *Electrocatal. Oxygen Reduct. React.* (2008) 89–134.
- [2] Q. Wei, Y. Fu, G. Zhang, S. Sun, *Curr. Opin. Electrochem.* 4 (2017) 45–59.
- [3] J. Healy, C. Hayden, T. Xie, K. Olson, R. Waldo, M. Brundage, H. Gasteiger, J. Abbott, *Fuel Cells* 5 (2005) 302–308.
- [4] X. Ge, A. Sumboja, D. Wu, T. An, B. Li, F.W.T. Goh, T.S.A. Hor, Y. Zong, Z. Liu, *ACS Catal.* 5 (8) (2015) 4643–4667.
- [5] Q. Ly, B.V. Merinov, H. Xiao, W.A. Goddard, T.H. Yu, *J. Phys. Chem. C* 121 (44) (2017) 24408–24417.
- [6] M. Winter, R.J. Brodd, *Chem. Rev.* 104 (10) (2004) 4245–4270.
- [7] X. Cui, S. Yang, X. Yan, J. Leng, S. Shuang, P.M. Ajayan, Z. Zhang, *Adv. Funct. Mater.* 26 (31) (2016) 5708–5717.
- [8] L. Jin-Cheng, H. Peng-Xiang, L. Chang, *Small* 13 (45) (2017) pp. 1702002.
- [9] J. Zhang, Z. Xia, L. Dai, *Sci. Adv.* (7) (2015) 1.
- [10] Q. Wei, G. Zhang, X. Yang, R. Chenitz, D. Banham, L. Yang, S. Ye, S. Knights, S. Sun, *ACS Appl. Mater. Interfaces* 9 (42) (2017) 36944–36954.
- [11] K. Gong, F. Du, Z. Xia, M. Durstock, L. Dai, *Science* 323 (5915) (2009) 760–764.
- [12] L. Dai, Y. Xue, L. Qu, H.-J. Choi, J.-B. Baek, *Chem. Rev.* 115 (11) (2015) 4823–4892.
- [13] Z. Yao, J. Yan, J. Mietek, J. Yonggang, Q.S. Zhang, *Small* 8 (23) (2012) 3550–3566.
- [14] J. Benson, Q. Xu, P. Wang, Y. Shen, L. Sun, T. Wang, M. Li, P. Papakonstantinou, *ACS Appl. Mater. Interfaces* 6 (22) (2014) 19726–19736.
- [15] L. Qu, Y. Liu, J.-B. Baek, L. Dai, *ACS Nano* 4 (3) (2010) 1321–1326.
- [16] Z. Xuejun, Q. Jinli, Y. Lin, Z. Jiuju, *Adv. Energy Mater.* 4 (8) (2014) pp. 1301523.
- [17] X. Tong, Q. Wei, X. Zhan, G. Zhang, S. Sun, *Catalysts* 7 (2017) 1 p. 1.
- [18] L. Ziyin, W. Gordon, L. Yan, L. Meilin, W. Ching-Ping, *Adv. Energy Mater.* 2 (7) (2012) 884–888.
- [19] J. Wu, L. Ma, R.M. Yadav, Y. Yang, X. Zhang, R. Vajtai, J. Lou, P.M. Ajayan, *ACS Appl. Mater. Interfaces* 7 (27) (2015) 14763–14769.
- [20] Q. Wei, X. Tong, G. Zhang, J. Qiao, Q. Gong, S. Sun, *Catalysts* 5 (3) (2015) p. 1574.
- [21] W. Shuangyin, Z. Lipeng, X. Zhenhai, R. Ajit, C.D. Wook, B. Jong-Beom, D. Liming, *Angew. Chem. Int. Ed.* 51 (17) (2012) 4209–4212.
- [22] K. Parvez, R. Li, S.R. Punirreddy, Y. Hernandez, F. Hinkel, S. Wang, X. Feng, K. Müllen, *ACS Nano* 7 (4) (2013) 3598–3606.
- [23] J.M. Munuera, J.I. Paredes, M. Entrerría, A. Pagán, S. Villar-Rodil, M.F.R. Pereira, J.I. Martins, J.L. Figueiredo, J.L. Cenís, A. Martínez-Alonso, J.M.D. Tascón, *ACS Appl. Mater. Interfaces* 9 (28) (2017) 24085–24099.
- [24] L. Na, L. Fang, W. Haoxi, L. Yinghui, Z. Chao, C. Ji, *Adv. Funct. Mater.* 18 (10) (2008) 1518–1525.
- [25] C.-Y. Su, A.-Y. Lu, Y. Xu, F.-R. Chen, A.N. Khlobystov, L.-J. Li, *ACS Nano* 5 (3) (2011) 2332–2339.
- [26] I.-Y. Jeon, H.-J. Choi, S.-M. Jung, J.-M. Seo, M.-J. Kim, L. Dai, J.-B. Baek, *J. Am. Chem. Soc.* 135 (4) (2013) 1386–1393.
- [27] K. Parvez, Z.-S. Wu, R. Li, X. Liu, R. Graf, X. Feng, K. Müllen, *J. Am. Chem. Soc.* 136 (16) (2014) 6083–6091.
- [28] S. Yang, S. Brüller, Z.-S. Wu, Z. Liu, K. Parvez, R. Dong, F. Richard, P. Samori, X. Feng, K. Müllen, *J. Am. Chem. Soc.* 137 (43) (2015) 13927–13932.
- [29] A.M. Abdelkader, I.A. Kinloch, R.A.W. Dryfe, *ACS Appl. Mater. Interfaces* 6 (3) (2014) 1632–1639.
- [30] G. Wang, J. Yang, J. Park, X. Gou, B. Wang, H. Liu, J. Yao, *J. Phys. Chem. C* 112 (22) (2008) 8192–8195.
- [31] D. Li, M.B. Müller, S. Gilje, R.B. Kaner, G.G. Wallace, *Nat. Nanotechnol.* 3 (2008) p. 101.
- [32] A. Ganguly, S. Sharma, P. Papakonstantinou, J. Hamilton, *J. Phys. Chem. C* 115 (34) (2011) 17009–17019.
- [33] S. Saxena, T.A. Tyson, S. Shukla, E. Negusse, H. Chen, J. Bai, *Appl. Phys. Lett.* 99 (1) (2011) p. 013104.
- [34] K. Parvez, Z.-S. Wu, R. Li, X. Liu, R. Graf, X. Feng, K. Müllen, *J. Am. Chem. Soc.* 136 (2014) 6083–6091.
- [35] K. Parvez, R. Li, S.R. Punirreddy, Y. Hernandez, F. Hinkel, S. Wang, X. Feng, Klaus Müllen, *ACS Nano* 7 (4) (2013) 3598–3606.
- [36] I.S. Flyagina, K.J. Hughes, D.C. Mielczarek, D.B. Ingham, M. Pourkashanian, *Fuel Cells* 16 (5) (2016) 568–576.
- [37] J. Wu, L. Ma, R.M. Yadav, Y. Yang, X. Zhang, R. Vajtai, J. Lou, P.M. Ajayan, *ACS Appl. Mater. Interfaces* 7 (2015) 14763–14769.
- [38] T. Xing, Y. Zheng, L.H. Li, B.C.C. Cowie, D. Gunzelmann, Qiao, Shi Zhang, S. Huang, Y. Chen, *ACS Nano* 8 (7) (2014) 6856–6862.
- [39] L. Wang, Z. Sofer, A. Ambrosi, P. Šimek, M. Pumera, *Electrochim. commun.* 46 (2014) 148–151.
- [40] Z. Lin, G.H. Waller, Y. Liu, M. Liu, C.-p. Wong, *Nano Energy* 2 (2) (2013) 241–248.
- [41] D. Deng, L. Yu, X. Pan, S. Wang, X. Chen, P. Hu, L. Sun, X. Bao, *Chem. Commun.* 47 (36) (2011) 10016–10018.
- [42] S.K. Bikkarolla, P. Cumpson, P. Joseph, P. Papakonstantinou, *Faraday Discuss.* 173 (0) (2014) 415–428.
- [43] K. Parvez, S. Yang, Y. Hernandez, A. Winter, A. Turchanin, X. Feng, K. Müllen, *ACS Nano* 6 (11) (2012) 9541–9550.
- [44] W. Yuan, Y. Zhou, Y. Li, C. Li, H. Peng, J. Zhang, Z. Liu, L. Dai, G. Shi, *Sci. Rep.* 3 (2013) 2248.
- [45] T. Ikeda, Z. Hou, G.-L. Chai, K. Terakura, *J. Phys. Chem. C* 118 (31) (2014) 17616–17625.
- [46] Z. Xu, X. Fan, H. Li, H. Fu, W.M. Lau, X. Zhao, *Phys. Chem. Chem. Phys.* 19 (31) (2017) 21003–21011.
- [47] S.T. Hossain, R. Wang, *Electrochim. Acta* 216 (2016) 253–260.